ACS Sustainable Chemistry & Engineering

Research Article

pubs.acs.org/journal/ascecg

ZnO-Based Imine-Linked Coupled Biocompatible Chemosensor for Nanomolar Detection of Co^{2+}

Hemant Sharma,[†] Ajnesh Singh,[†] Navneet Kaur,*[,‡] and Narinder Singh*[,†]

[†]Department of Chemistry, Indian Institute of Technology Ropar (IIT Ropar), Rupnagar, Panjab, India 140001

[‡]Centre for Nanoscience and Nanotechnology (UIEAST), Panjab University, Chandigarh, India 160014

Supporting Information

ABSTRACT: A sol–gel process is developed for the synthesis of ZnO crystals at room temperature using organic receptors (bearing imine linkages) as the capping agents to control the size and shape of ZnO. The size and morphology of ZnO are characterized with X-ray diffraction, TEM, SEM, and DLS studies. The decoration of imine-linked receptors on the surface of ZnO is characterized with IR and NMR spectroscopy and confirmed with EDX analysis. The XRD results show that the average crystallite size of ZnO is 13.8 nm with a hexagonal wurtzite structure. Fluorescence spectroscopy revealed that surface-coated ZnO possesses fewer surface defects than the usual bulk ZnO. The imine-linked receptor-coated ZnO (sensor) was tested for recognition of various metal ions; however, the sensor was found to be selective for Co^{2+} in the DMSO/H_2O (8:2; v/v) solvent system. The successive addition of Co^{2+} to the solution of the sensor quenches the fluorescence intensity at 445 nm with enhancement at 353 nm. This leads to the development of a ratiometric fluorescence sensor for the recognition of Co^{2+} in a semi-aqueous solvent system with a detection limit of 0.4 nM. To the best of our knowledge, this manuscript represents the first ZnO-based imine-linked coupled biocompatible chemosensor for nanomolar detection of Co^{2+}.

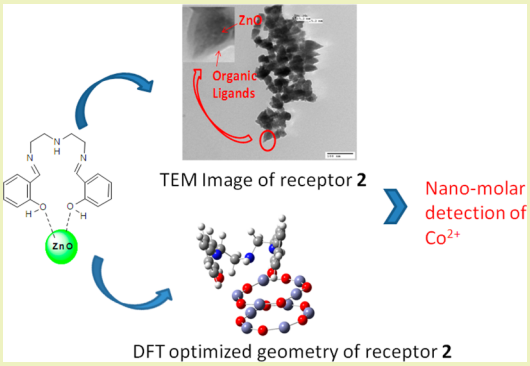

KEYWORDS: *ZnO, Ratiometric, Surface decoration, Fluorescent detection, Cobalt*

INTRODUCTION

The development of chemosensors for the recognition and estimation of transition metal ions in a water sample is of great interest.[1,2] The determination of transition metal ions in environmentally and biologically important samples is generally required as the transition metal ions are a paradox to life. A trace amount of several transition metal ions is required in many cellular processes, and many enzymatic reactions are under the direct control of these metal ions.[3] However, exposure to transition metal compounds have been associated with adverse health effects, including allergic and autoimmune diseases.[4,5] The research arena focused on the development of new fluorescent molecules is attracting interest,[6,7] and particularly, the ZnO-based chemosensors are emerging as an interesting field as this semiconductor material has excellent optical and electronic properties, encompassing a wide band gap (3.37 eV) and a high exciton binding energy of 60 meV.[8] These unique physical and chemical properties arise from quantum-sized effects and make quantum-sized ZnO an interesting material for chemosensors.[9] Many literature reports describe gas sensing with ZnO;[10,11] however, there are few ZnO-based receptors available for cation recognition.[12−16] It is well established that the sensing properties are dependent on size, crystalline structure, and morphology of the ZnO.[17−19] In addition to these, the capping agent can also affect the sensing properties of system.[12−15,20] In the last decades, several methods have been developed for the synthesis of quantum-sized ZnO.[21,22] The sol–gel route is the most favorite and successful approach because it is cheap and efficient and has relatively less harsh condition requirements. Contrary to these advantages for ZnO synthesis, the sol–gel process has one major drawback as the colloidal ZnO nanoparticles thus obtained tend to aggregate or may undergo Ostwald ripening due to their small size and high surface energy. Recently, using high surface area support, the preparation of nonagglomerated nanometer-sized particles have been reported.[23] Along the same lines, the quantum size of ZnO can be stabilized by using capping agents.[24] Receptors bearing carboxylic acid (−COOH), thiol (−SH), and amine (−NH2) function groups are used as capping agents. On the basis of the HSAB principle and available reports of imine-linked receptors for Zn^{2+} recognition, we contemplate using a new class of imine-linked receptors to control the size of ZnO.[15,25,26] The imine-linked receptor is expected to adsorb on the surface of ZnO, and this strategy has a second advantage as the imine linkages of the resultant sensor (ZnO coated with an imine-linked receptor) may offer additional binding sites for the recognition of metal ions.

Received: July 25, 2013
Revised: September 10, 2013
Published: September 17, 2013

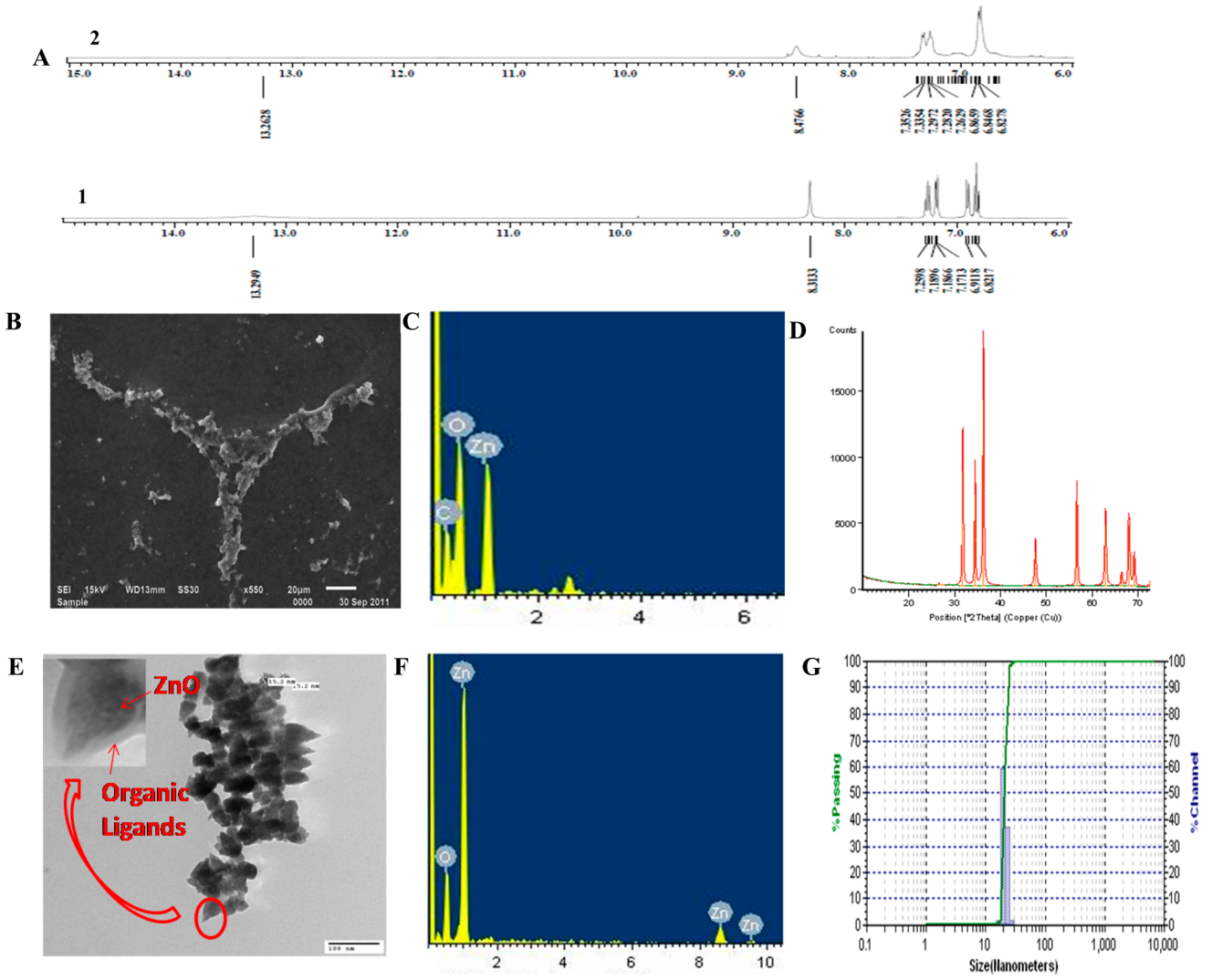

Figure 1. (A) Comparison of partial ^{1}H NMR spectrum of **1** and **2**. (B) SEM image of compound **2**, showing a tripodal growth of self-assembled structure due to the structure directing nature of compound. (C) EDX analysis of compound **2** (as prepared) showing the coatings of organic molecules on ZnO. (D) X-ray powder diffractogram of ZnO (obtained by heating compound **2** at 500 °C for 3 h.) (E) TEM image of compound **2** (showing average particle size of 15.2 nm) and inset clearly shows coating of organic ligand on ZnO. (F) EDX analysis of compound **2** after heating at 500 °C for 1 h, showing the presence of ZnO. (G) Size distribution study of **2** (representing the hydrodynamic diameter of 20 nm).

EXPERIMENTAL SECTION

Materials and Methods. Fourier transform infrared (FT-IR) spectra of **1** and **2** were recorded using a Bruker Tensor 27 spectrometer in a range from 600 to 4000 cm^{-1}. The NMR spectra of **1** and **2** were recorded in $CDCl_3$/DMSO-d_6 solvent with TMS as an internal reference on a JNM-ECS400 (JEOl) spectrophotometer; which operated at 400 MHz for ^{1}H NMR spectra. The crystal structure of the ZnO powders were analyzed by X-ray diffraction (XRD) with a PANalytical X'PERT PRO diffractometer operated at 45 KV and 40 mA using Ni-filtered Cu Kα radiations with a scan speed of 10°/min for 2θ in a range from 10 to 75. For measurement, an air-dried fine powder was taken and made a uniform layer on a zero background sample holder. The average crystalline size was estimated by Debye–Scherrer's equation using XRD analysis data.[27] The morphology and elemental (EDX) analysis were performed on a scanning electron microscope (SEM JEOL JSM-6610LV) using a voltage of 15 KV. For SEM analysis, the samples were prepared by dispersing ZnO in ethanol, and a drop of dilute ZnO solution (100 μM) was deposited on carbon tape and dried at room temperature under vacuum. The size distribution of ZnO particles was determined on a Metrohm Microtrac Ultra Nanotrac particle size analyzer (dynamic light scattering) using a DMSO/H_2O (8:2, v/v) system as the dispersion medium, and three readings were recorded per sample. The UV–vis absorption spectra were obtained on a Specord 250 Plus Analytikjena spectrophotometer using quartz cells having a 1 cm path length, and solid state absorption spectra were obtained by using quartz plates coated with a fine coating of material. The photoluminescence measurements were carried on a Perkin-Elmer L55 spectrofluorimeter with a scanning speed of 400; the excitation and emission slit width was 10 nm. A special solid-state assembly was used to record the solid-state photoluminescence, having a quartz plate fitted sample holder. The electrochemical measurements were recorded on potentiostat-galvanostat BASI EPSILON. All electrochemical measurements were performed in a single-compartment cell under a nitrogen atmosphere at 25 °C worked with Pt disk working electrode, platinum wire counter electrode, and Ag/$AgNO_3$ reference electrode. Tetrabutylammoniumhexafluorophosphate was used as the supporting electrolyte. TEM images were recorded on a Hitachi (H-7500) instrument worked at 80 KV. A 400-mesh carbon-coated copper grid was used for sample preparation. The modified ZnO nanoparticles were suspended in ethanol. A drop of solution is placed onto the grid, and excess solvent is drawn off after 1 min. The surface area was calculated using an Autosorb-IQ Quantachrome Instruments volumetric adsorption analyzer. The samples were degassed at 200 °C under vacuum for 3 h. The Brunauer–Emmett–

dx.doi.org/10.1021/sc400250s | ACS Sustainable Chem. Eng. 2013, 1, 1600–1608

Teller (BET) model from a linear part of BET plot (P/PO: 0.05−0.3) was employed for surface area calculation.

Synthesis of Imine-Linked Receptor and Decoration on ZnO. All chemical reagents were analytical grade and were used without further purification. Imine-linked receptor **1** was synthesized by the condensation reaction between diethylene triamine (100 mg, 1.0 mmol) and salicylaldehyde (295 mg, 2.4 mmol) in dry ethanol. The reaction mixture was stirred at room temperature for 5 h. A yellow colored product **1** separated out. This product was filtered and washed with cold ethanol. The structure elucidation data of **1** matched with the literature report.[28] IR (KBr): ν_{max} (in cm^{-1}) 1630 (C═N), 1459 (CH_2); ^{1}H NMR δ(ppm) 13.29 (bs, 2H, OH), 8.31 (s, 2H, N═CH), 7.23 (t, 2H, ArH), 7.18 (d, 2H, ArH), 6.91 (d, 2H, ArH), 6.82 (t, 2H, ArH), 3.67 (m, 4H,═NCH2), 2.95 (m, 4H, NCH2); ^{13}C NMR δ(ppm) 165.9, 161.0,132.2, 131.2, 118.6, 118.4, 116.8, 59.3, 49.5; CHN Analysis; Calcd. C, 69.43; H, 6.80; N, 13.49; Found C, 69.78; H, 6.53; N,13.27. The quantum-sized ZnO crystals were synthesized by taking $Zn(ClO_4)_2{\cdot}6H_2O$ (750 mg, 2.0 mmol) along with receptor **1** (925 mg, 3.0 mmol) in dry ethanol (25 mL). The solution was maintained at constant stirring with a solution temperature of 25 °C.The NaOH solution was slowly added to the Zn^{2+} solution dropwise. The stirring of solution was continued for 2 h, and a dispersion of ZnO particles gradually formed in the solution. The as-prepared dispersion was centrifugally filtered and washed with ethanol and deionized distilled water five times. Product **2** was dried at 50 °C for 24 h. IR (KBr): ν_{max} (in cm^{-1}) 1643 (C═N); ^{1}H NMR δ(ppm) 13.26 (bs, 2H, OH), 8.47 (bs, 2H, N═CH), 7.29 (m, 4H, ArH), 6.84 (m, 4H, ArH), 3.61 (m, 4H, ═NCH_2), 2.71 (m, 4H, NCH_2); ^{13}C NMR δ(ppm) 166.4, 160.8, 132.1, 131.4, 118.6, 118.2, 116.4, 58.2, 49.4. A small sample of **2** was kept at 500 °C for 2 h to burn the organic receptor coated on the surface of ZnO. The bulk ZnO was obtained by the literature method.[20]

Metal Ion Recognition Properties of 1 and 2. All the recognition studies were carried out at 25 ± 1 °C, and before recording any spectrum, an adequate time was provided with shaking to ensure the uniformity of the solution. The cation binding behavior of **1** and **2** toward different cations, including Na^+, K^+, Mg^{2+}, Sr^{2+}, Ba^{2+}, Cr^{3+}, Mn^{2+}, Fe^{3+}, Co^{2+}, Ni^{2+}, Cu^{2+}, Zn^{2+}, Ag^+, Cd^{2+}, Hg^{2+}, Pb^{2+}, and Al^{3+}, was investigated through the changes in fluorescence spectra of **1** and **2**. The metal binding tests of **1** and **2** were performed by mixing standard solutions of the sensor (10 nM) along with fixed amounts of a particular metal nitrate salt (50 nM in HEPES-buffered in DMSO/H_2O (8:2, v/v). The fluorescence spectra of **1** and **2** were recorded with excitation wavelengths shown in the respective figures. The titration was performed with a standard solution of assembly **2** (15 nM) along with consecutive addition of cobalt nitrate (0−50 nM) in HEPES-buffered DMSO/H_2O (8:2, v/v). To evaluate any possible interference due to other cations for the estimation of Co^{2+}, solutions were prepared containing **2** (10 nM) and Co^{2+} (50 nM) along with and without other interfering metal ions (50 nM) in DMSO/H_2O (8:2, v/v) HEPES-buffered solution (pH 7.0 ± 0.1). The size distributions of the complex formed between **2** and a Co^{2+} in DMSO/H_2O (8:2, v/v) system were recorded using dynamic light scattering (DLS)-based particle size analyzer. To understand the changes in the redox potential of Co^{2+} upon addition of receptor **2**, the titration was performed on a cyclic voltammeter using a stock solution of cobalt nitrate together with the successive addition of sensor **2** in HEPES-buffered DMSO/H_2O (8:2, v/v), and tetrabutylammoniumhexafluorophosphate (0.01 M) was used as the supporting electrolyte.

Cytotoxicity of 2. The osteosarcoma cell line KHOS-NP having a density of 1.0 × 10^5 cells/mL was employed for evaluation of cytotoxicity of **2**, and it was monitored using the 3-(4,5-dimethyl-2-thiazolyl)-2,5-diphenyl-2H-tetrazolium bromide (MTT) assay. The cell line is cultured in a 96-well flat-bottomed microplate in growth media (200 μL) along with different concentrations of **2** and incubated at 37 °C under a 5% CO_2 atmosphere for 2 days. After that, a 10 μL solution of MTT (5 mg/mL) was added to each well and mixed properly with shaking. This plate was again allowed to incubate at 37 °C under a 5% CO_2 atmosphere for 2 h. The media was removed, and 100 μL of DMSO was added to each well. Following mixing, the absorbance spectrum of each solution was recorded at 560 nm.

RESULTS AND DISCUSSION

The IR spectrum of imine-linked receptor **1** exhibits a band at 1630 cm^{-1} due to the stretching of imine linkage (−CH═N). The peaks at 1459 cm^{-1} are attributed to the bending vibrations of $-CH_2$ group (Figure S1, Supporting Information). The ^{1}H and ^{13}C NMR spectrum of **1** showing signals for imine linkage (−CH═N) at δ8.31 and δ165.9 further validates the structure (Figure 1A and Figures S2 and S3, Supporting Information). The elemental analysis also favors the chemical formula of receptor **1** shown in Scheme 1. The solid state of **1** exhibited an

Scheme 1

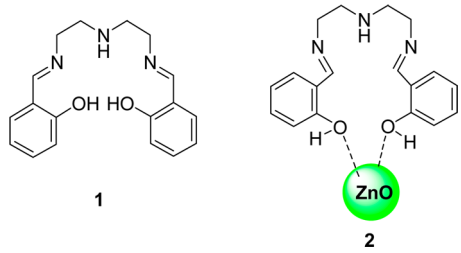

absorption band at 410 nm, a characteristic band of imine linkages (Figure S6, Supporting Information). Upon excitation of a solid sample of **1** at 410 nm, an emission band was observed at 486 nm (Figure S7, Supporting Information). The IR spectra of **2** exhibited a band at 1643 cm^{-1}, which is assigned as the band due to imine linkages of organic receptor-coated on ZnO (Figure S1, Supporting Information). There are three possibilities of decoration of **1** on a ZnO surface as shown in Scheme S1 of the Supporting Information. A comparison of ^{1}H NMR spectra (Figure 1A) of **1** and **2** revealed the shifts in the signals responsible for −OH and (−CH═N), which was minute for −OH ($\Delta\delta$ = 0.03) and notable for −CH═N ($\Delta\delta$ = 0.16). Broadening of all signals also substantiate the binding of receptor **1** on the surface of ZnO. On the basis of DLS analysis (Figure 1G), the hydrodynamic diameter of particles was calculated to be 20 nm. Concurrent evidence of NMR and DLS analysis favors the formation of the structure shown as A in Scheme S1 of the Supporting Information.[14] The possibility of B and C is ruled out because if B is the structure then each ^{1}H NMR signal responsible for −OH, CH═N, Ar, and CH_2 must split into two or more. On the other hand, if there is structure C, then particle size must grow to an appreciable extent. The presence of **1** during the synthesis of ZnO caused the growth of ZnO in particular directions, thus leading to the formation of a tripodal geometry, as shown in Figure 1B and Figure S8 of the Supporting Information, and ascertaining the special binding behavior of **1**.

It is well established in the literature that the presence of capping agents may direct the growth of ZnO in a particular direction.[12−15,20] The structure-directing agents (SDAs) are widely used in research and industry to control the size and shape of particles. In the case of metal nanoparticles, SDAs such as surfactants, phospholipids, proteins, and other polymeric materials can control their shape. Such SDAs have been reported to control the shape of QDs as well.[29−31] There are various examples in the literature citing the effect of change of SDAs; the porosity of material was changed and lead to good catalytic activity, e.g., pores and channels of zeolites.[32,33] Most

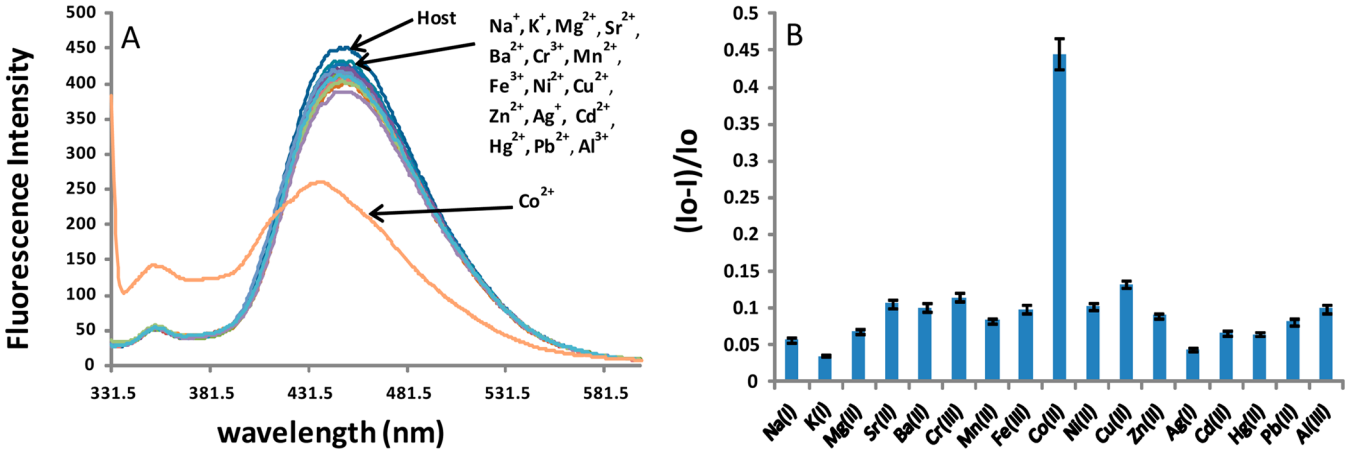

Figure 2. (A) Changes influorescence intensity of **2** (10 nM) upon addition of 50 nM of a particular metal nitrate salt in a HEPES-buffered DMSO/H_2O (8:2, v/v) solvent system (excitation at 325 nm). (B) Normalized fluorescence intensity ($I_o - I/I_o$) of **2** (10 nM) at 445 nm upon addition of 50 nM of a particular metal nitrate salt in HEPES-buffered DMSO/H_2O (8:2, v/v). The reported values represent the outcomes of three independent determinations.

of applications of SDAs are reported in catalysis, and for the first time, our group explored its use in sensing of metal.[14] In the present study, the simple organic imine-linked receptor was employed as a SDA, which controls the shape of ZnO nanoparticles. The SEM images illustrated that modified ZnO nanoparticles form supramolecular self-assembled structures with growth limited in particular directions and thereby generating tripodal geometry (Figure 1B and and Figure S8, Supporting Information). The EDX analysis of **2** shows the presence of an organic part along with ZnO (Figure 1C and Figure S9A, Supporting Information). An air-burnt sample of **2** shows the presence of only ZnO (Figure 1F and Figure S9B, Supporting Information). This clearly confirms the coating of an organic receptor on the surface of ZnO, which burns out to provide ZnO, the elemental composition of complex **2**. Co^{2+} was also confirmed through the EDX analysis as shown in Figure S9C of the Supporting Information. Figure 1D shows the X-ray powder diffraction pattern of ZnO crystals calcinated at 500 °C, showing scattering angles (2θ) of 31.5, 34.7, 36.1, 47.4, 56.5, 62.7, and 67.8 corresponding to the reflections from 100, 002, 101, 102, 110, 103, and 112 crystal planes, respectively. All diffraction peaks are in good agreement with literature reports, which can be indexed as the hexagonal wurtzite structure of ZnO with lattice constants of a = 3.253 Å and c = 5.20 Å. No other peak (except assigned for ZnO) was observed, confirming the purity in the samples. The peak broadness can be used as a measure to determine the average crystalline size (D) by using Debye−Scherrer's equation ($D = 0.89\lambda/\mathrm{B}\cos\theta$), where λ is the X-ray wavelength (0.154 nm); θ is the Bragg diffraction angle; and B is the width at half-maximum of diffraction peak (FWHW). The average crystalline size of the ZnO nanocrystals is estimated to be 13.8 nm. The size is determined by assuming that the strains and faulting are ignored, and peak broadening is only due to the crystalline domain size and distribution. It is important to mention here that the peak broadening in the diffraction patterns mainly consists of the following factors: (a) microstrains (deformations of the lattice), (b) faulting (extended defects), (c) crystalline domain size, and (d) domain size distribution. The thickness of coated nanoparticles was characterized with dynamic light scattering (DLS), which records the hydrodynamic diameter of the coated nanoparticles. It was observed that there is a difference in size measured by TEM, AFM, and DLS because dynamic light scattering (DLS) measures the hydrodynamic size and is a more reliable technique to measure the size of coated nanoparticles. The coated materials cause a significant frictional drag that can influence the Brownian motion of particle.[34] However, particle agglomeration can cause a significant drift in the DLS-measured size. Therefore, TEM is necessary to ensure that the size measured by DLS represents the size of a discrete particle and not the size of an agglomerate.[35] The TEM images of assembly **2** (Figure 1E) ensure the nanometer dimensions of ZnO nanoparticles (about 15.2 nm). The inset of Figure 1E also shows the presence of an organic coating on the surface of the ZnO nanoparticles. The TEM image of **2** additionally depicts that the grain boundaries of the imine-linked receptor-coated ZnO are of large size and inclined to each other, which otherwise are not observed in pure ZnO produced under the same reaction conditions except when using the imine-linked receptor. Various applications of ferromagnetic nanostructured ZnO rely upon the grain boundaries of doped ZnO such as in spintronics.[36−38] Comparing the effect of these grain boundaries of nanocrystalline material with conventional coarse-grained polycrystalline materials, it is more obvious in nanocrystalline materials due to a larger volume fraction of atoms lying at grain boundaries. The solid state UV−vis absorption spectra of pure ZnO exhibit a peak at 360 nm corresponding to the exciton state of ZnO (Figure S6, Supporting Information). The λ_{max} of the absorption spectra of **2** was red-shifted as compared to that of pure ZnO.[39] The photoluminescence measurements were performed at an excitation wavelength of 325 nm. The fluorescence spectra of pure ZnO exhibited bands at 434 and 456 and a broad green emission band at 520 nm. According to Dijken et al. the visible emission band is explained on the basis of formation of a recombination center (Vo**), where the valence band hole is trapped by the surface state and then tunnels back into oxygen vacancies containing one electron (Vo*).[40] This recombination of a shallow trapped electron with a deeply trapped hole in a Vo** center is responsible for visible emission. The solid-state photoluminescence spectra of receptor-coated ZnO shows enhancement in intensity at 434 and 456 nm (as of pure ZnO); however, intensity at 520 nm quenched as compared to pure ZnO. The explanation of this

effect lies in the fact that in pure ZnO nanoparticles, huge surface defects exist, which result in intense visible emissions (Figure S7, Supporting Information).

The oxygenated zinc defects at the grain boundaries of ZnO may facilitate the conjugation with −OH and −CH═N groups of receptor **1**. As a result, the interface defects decrease in receptor-coated ZnO (**2**), and the probability of a surface-trapped hole is decreased. At the same time, **1** spatially blocks the process of a surface-trapped hole tunneling back into the particles to form a Vo** center. Both effects lead to a decrease in the probability of a Vo** recombination and explain less intense visible emissions from the receptor-capped ZnO as compared to pure ZnO. Apart from decreasing the interface defects of ZnO, the coating of the organic receptor on the surface of ZnO leads to selectivity. The selectivity is raised due to a combination of two factors: (a) a hindered free rotation of the molecule and (b) an increase in surface area to volume ratio. The receptor alone has a nonselective profile due to free rotation around the single−single bond. The ZnO particle has strong affinity toward the hydroxyl group. Therefore, the coating restricts the free rotation of the receptor molecule and produces a prominent cavity for a metal cation (Scheme 1).[14] Further, the surface area of the ZnO nanoparticles before and after coating is characterized by BET. It was found that coated ZnO nanoparticles have more surface area (118.28 m^2/g) as compared to bare ZnO nanoparticles (21.24 m^2/g) as shown in Figure S10 of the Supporting Information. It is believed that there is a direct relation between sensor activity and the surface area of the sensor because with an increase in surface area the number of binding sites per unit volume increase, which proved immediate and in close contact with analyte and leads to high sensitivity, low detection limit, and small response time. The fluorescence spectra of **2** recorded in a HEPES-buffered DMSO/H_2O (8:2, v/v) solvent system is completely different from the solid-state spectra of **2** (Figure 2A). Literature reports have demonstrated that the solid-state fluorescence spectra may differ from the spectra of the sample dissolved in some solvent.[41] Moreover, the solvent polarity may also influence the fluorescence signature of any sample. Therefore, a solvatochromic study was performed by recording the absorbance and emission spectra of receptor **2** in four different solvents (DMF, $CHCl_3$, CH_3CN, and DMSO) shown in Figure S15 of the Supporting Information. Figure S15A of the Supporting Information showed that there is no significant change in the absorption profile of **2** in a different solvent. However, emission spectra were almost the same, except in the case of DMF and DMSO, where a new band was originated at 370 nm. The possible cause behind this new band was the interaction of these high polarity solvents with receptor **2** (Figure S15B, Supporting Information). The emission band (λ_{max} = 445 nm) of **2** (10 nM) recorded in HEPES-buffered DMSO/H_2O (8:2, v/v) was blue-shifted in contrast to the emission band observed in the solid-state fluorescence spectrum of **2**. However, both were excited at the same wavelength (λ_{ext} = 325 nm). The fluorescence spectrum of **1** also showed a similar band, indicating that the observed band is characteristic of imine linkages (Figure S11, Supporting Information). To represent the imine linkage, absorption spectra of diethylene triamine, salicylaldehyde, and receptor **1** are recorded in DMSO as shown in Figure S16 of the Supporting Information. It is observed that receptor **1** has a band in the visible region, and it is neither shown by amine nor by aldehyde, which is the characteristic band of the imine (−CH═N) linkage. The changes in fluorescence intensity of **2** upon addition of different metal salts were recorded (Figure 2A), and it was found that the addition of Co^{2+} salt (50 nM) to the solution of compound **2** (10 nM) resulted in quenching in intensity at 445 nm and emergence of a band at 353 nm. Under the same conditions, addition of any other metal ion (such as Na^+, K^+, Mg^{2+}, Sr^{2+}, Ba^{2+}, Cr^{3+}, Mn^{2+}, Fe^{3+}, Ni^{2+}, Cu^{2+}, Zn^{2+}, Ag^+, Cd^{2+}, Hg^{2+}, Pb^{2+}, and Al^{3+}) did not show such a significant change in the fluorescence profile of **2**. Cobalt has an indispensable role in biological systems, such as being a stimulant for the production of red blood cells and the main constituent of vitamin B12, which is involved in normal physiological functioning of the brain and nervous system.[42−44] It is also involved in metabolism of every cell of human body and in the synthesis of protein and fatty acids.[42,43] Besides, it also has some pestilential effects on human health, for example, anemia, damage to the nervous system, and loss of appetite.[45] Hence, determination of the Co^{2+} level in biological and water samples is essential, and many efforts are devoted in this direction (Table S1, Supporting Information). Leng et al. used the modified gold nanoparticles for the colorimetric estimation of Co^{2+}.[49] Cannizzaro et al. reported the lowest detection limit of 5 pM by using flow injection-chemiluminescence,[54] and some other sensors are also enlisted in Table S1, Supporting Information.[46−56] However, issues related to interference from other metal ions and biocompatibility of the sensor are not addressed. The fluorescence technique has more sensitivity as compared to other spectrophotometric methods. However, only few fluorophores are reported in the literature for the detection of Co^{2+}. This is the possible cause behind the need for oxidizing agents and the basic medium for passionate fluorescence response.[57] Here, we report a nanomolar detection of Co^{2+} by using a simple analysis system with high selectivity in biological fluids. In order to prove that imine-linked receptor **1** when coated on a ZnO surface is responsible for selectivity in recognition of Co^{2+}, the comparison of the fluorescence recognition properties of **2** with **1** and ZnO both individually and collectively is studied. A 10 μM solution of **1** in HEPES-buffered DMSO/H_2O (8:2, v/v) was mixed with 50 nM of metal ions (such as Na^+, K^+, Mg^{2+}, Sr^{2+}, Ba^{2+}, Cr^{3+}, Mn^{2+}, Fe^{3+}, Co^{2+}, Ni^{2+}, Cu^{2+}, Zn^{2+}, Ag^+, Cd^{2+}, Hg^{2+}, Pb^{2+}, and Al^{3+}), and it was found that no metal ions can modulate the fluorescence intensity of **1** both in terms of intensity and shift in the emission band (Figure S11, Supporting Information). Thus, it is concluded that free receptor **1** has no selectivity. Similarly, a metal binding test was performed using ZnO as the receptor site. ZnO was dissolved in HEPES-buffered DMSO/H_2O (8:2, v/v), and then 50 nM solution of Co^{2+} was added to it.

Interestingly, no change in the fluorescence signature of ZnO was observed (Figure S12, Supporting Information). This is quite expected, as the ZnO surface has no metal binding site. Encouraged with these results, we mixed a 1 nM solution of ZnO with a 1 nM solution of **1**, and the resultant solution was checked for metal binding assay. To our surprise, this event did not show any binding for the Co^{2+} ion (Figure S13, Supporting Information). Although, the solution has similar constituents as of **2**, these results suggest that if **1** is first decorated on the surface of ZnO, only then is the system selective for Co^{2+}, and under no other condition does the system have selectivity. The metal binding test with control receptors highlights the judicial choice and decoration of an organic receptor to fine tune the selectivity of a sensor for a particular metal ion. To gain more insight about the properties of **2** as a receptor for Co^{2+},

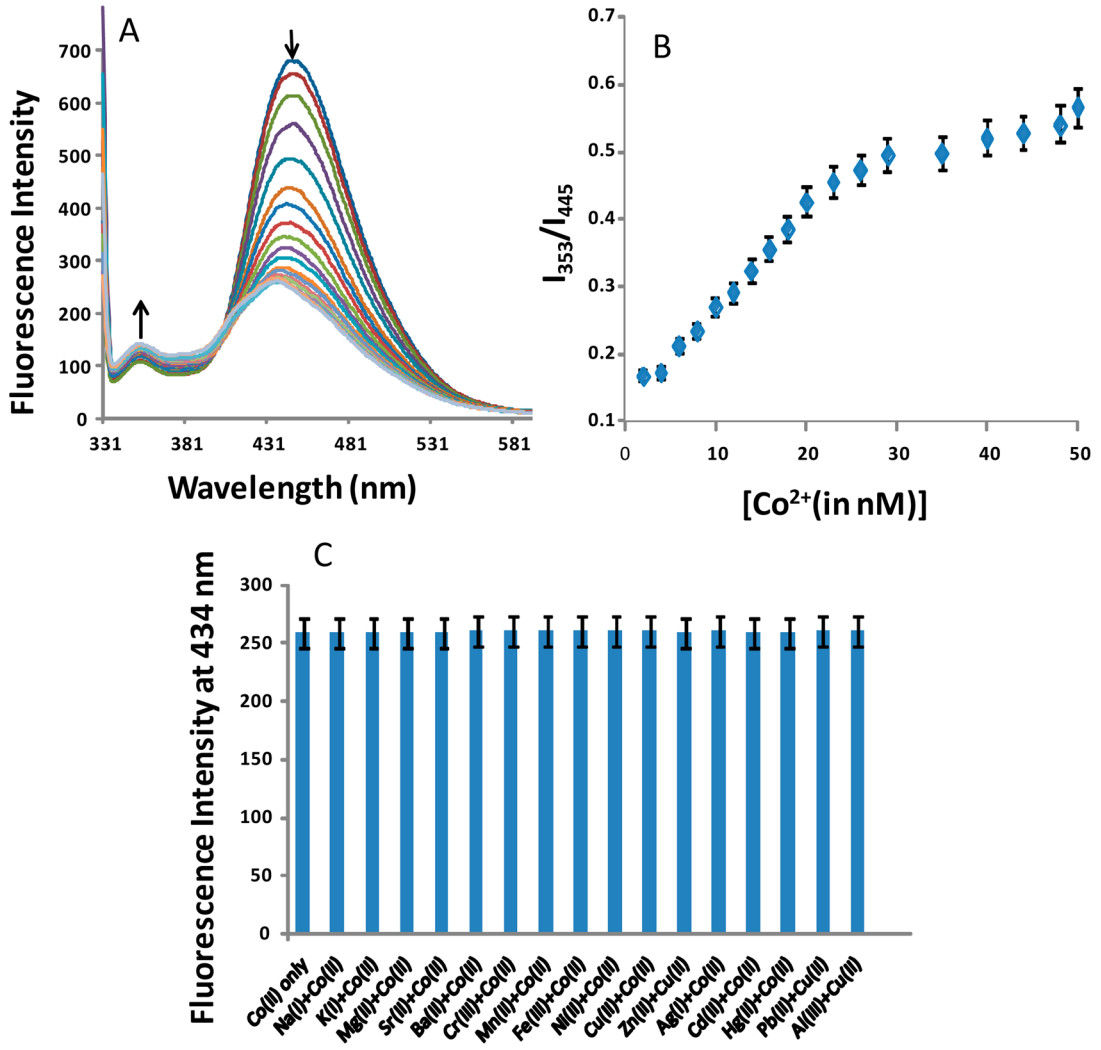

Figure 3. (A) Changes in fluorescence spectra of **2** (15 nM) upon successive addition of nitrate salt of Co^{2+} (0−50 nM) in HEPES-buffered DMSO/H_2O (8:2, v/v) (excitation at 325 nm). (B) Plot of ratiometric fluorescence intensity (I_{353} /I_{445}) of **2** (15 nM) against Co^{2+} concentration (0−50 nM) in HEPES-buffered DMSO/H_2O (8:2, v/v). The reported values represents the outcomes of three independent determinations. (C) Estimation of Co^{2+} in the presence of other metal ions (Na^+, K^+, Mg^{2+}, Sr^{2+}, Ba^{2+}, Cr^{3+}, Mn^{2+}, Fe^{3+}, Ni^{2+}, Cu^{2+}, Zn^{2+}.,Ag^+, Cd^{2+}, Hg^{2+}, Pb^{2+}, and Al^{3+}) in HEPES-buffered DMSO/H_2O (8:2, v/v).

fluorescence titration was carried out in HEPES-buffered DMSO/H_2O (8:2, v/v) by adding aliquots of Co^{2+} ion. The successive addition of Co^{2+} from 0−50 nM to receptor **2** resulted in a quenching and blue shift in emission band at 445 nm and enhancement at 353 nm (Figure 3A). The successive decrease in intensity at 445 nm and increase at 353 nm may authenticate the use of this receptor for the ratiometric estimation of Co^{2+}, and a plot between the ratiometric fluorescence intensity of **2** and concentration of Co^{2+} (0−25 nM) exhibits a linear relationship (Figure 3B).[58] The ratiometric estimation is always preferable over conventional detection because it is less sensitive to errors like photo-transformation, receptor concentration, and environmental effect.[58] To test the selectivity of compound **2** for Co^{2+}, competitive experiments were carried out in the presence of Co^{2+} (50 nM) mixed with one of the following metal ions: Na^+, K^+, Mg^{2+}, Sr^{2+}, Ba^{2+}, Cr^{3+}, Mn^{2+}, Fe^{3+}, Ni^{2+}, Cu^{2+}, Zn^{2+}, Ag^+, Cd^{2+}, Hg^{2+}, Pb^{2+}, or Al^{3+} (50 nM). As shown in Figure 3C, assembly **2** has a high selectivity for Co^{2+}, which is confirmed from comparing the fluorescence profile with and without other metal ions. Therefore, interference was not observed for the sensing of Co^{2+} with assembly **2** in the presence of other metal ions. Compiunds **1** and **2** were also examined for a change in absorption profile on the addition of various metal ions. Figure S14A of the Supporting Information represents the metal binding assay of receptor **1**, and it is found that no metal causes a change in the absorption profile of receptor **1** in a DMSO/H_2O (8:2, v/v) solvent system. The absorption spectra of **2** in aqueous DMSO/H_2O (8:2, v/v) displayed a broad absorption band centered at 330 nm, with an extinction coefficient ε_{max} = 3.8×10^3 $M^{-1}cm^{-1}$. Figure S14B of the Supporting Information shows that the UV−visible spectral response of **2** (10 nM) upon addition of some biologically important cations, such as Na^+, K^+, Mg^{2+}, Sr^{2+}, Ba^{2+}, Cr^{3+}, Mn^{2+}, Fe^{3+}, Co^{2+}, Ni^{2+}, Cu^{2+}, Zn^{2+}, Ag^+, Cd^{2+}, Hg^{2+}, Pb^{2+}, and Al^{3+}, displayed no significant binding. In order to examine the change in the redox behavior of receptor **2** on addition of Co^{2+}, the titration was performed on a cyclic voltammeter by using tetrabutylammoniumhexa-fluorophosphate (0.01 M) as the supporting electrolyte in a DMSO/H_2O (8:2, v/v) solvent system. It was found that titration between **2** and Co^{2+} results in an anodic shift (Figure 4).

dx.doi.org/10.1021/sc400250s | ACS Sustainable Chem. Eng. 2013, 1, 1600−1608

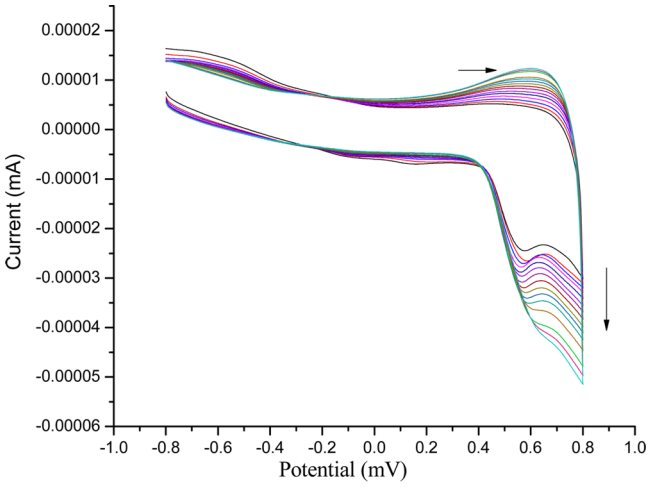

Figure 4. Changes in cyclic voltammogram as a result of titration between Co^{2+} and **2**. Reference electrode = $AgNO_3/Ag$; supporting electrolyte = $[n\text{-}Bu_4N]PF_6$. Scan rate = 100 mV/s.

In recent studies, DFT calculations have been performed to study the interactions and chemisorption of organic ligands on ZnO.[59,60] We hereby endeavored to investigate the binding of receptor **1** on the surface of ZnO that is responsible for selectivity for ion recognition by performing energy minimization studies. The small $(ZnO)_{10}$ cluster has been used to represent the ZnO nanoparticles. The energy minimized geometries for a small $(ZnO)_{10}$ cluster, receptor **1**, and a small $(ZnO)_{10}$ cluster with receptor **1** were obtained by using the B3LYP/6-311G basis set on Gaussian 09 program.[61] The optimized structure of $(ZnO)_{10}$ has a symmetric tubular geometry (Figure 5A). The nonselective profile of dipodal receptor **1** was also supported from its optimized geometry. Figure 5B revealed that dipodal receptor **1** does not have any definite cavity for the occupation of metal cations, which results in nonselective behavior of dipodal receptor **1**. In the case of a small $(ZnO)_{10}$ cluster with receptor **1** (a representative for assembly **2**), there is drastic change in the geometry of dipodal receptor **1**; both arms of the receptor came parallel and closer, which otherwise were perpendicular to each other in the isolated state via formation of Zn−O bonds between receptor **1** and the ZnO surface (Figure 5C).[60] Therefore, ZnO fixes its free rotation around a carbon−carbon single bond and offers a size-specific preorganized cavity for ion interaction. The energy of optimization also showed that a small $(ZnO)_{10}$ cluster with receptor **1** has more stability as compared to isolated receptor **1** (Table S2, Supporting Information).

The recognition of Co^{2+} in biological systems is essentially due to its numerous roles as already explained. Therefore, sensors should not disturb the normal homeostasis of a cell. In other words, sensors must exhibit compatibility with living systems. In this concern, the MTT assay was performed using the osteosarcoma cell line with standard conditions (incubation at 37 °C under a 5% CO_2 atmosphere for 2 days). The minimum concentration of receptor **2** required for recognition is 10 nM, which did not cause any cell lethality. To investigate the effect of a higher concentration, the dose dependent study was performed using different concentrations of receptor **2**. These results illustrate that 85% cell viability was observed up to a 5 μM concentration of receptor **2**.

CONCLUSIONS

An imine-linked receptor is used as a capping agent to control the size and shape of ZnO crystals. TEM, XRD, and DLS were used to ensure the size and coating on the surface of ZnO nanoparticles. Imine-linked receptor **1** is solely responsible for the shape, selectivity, and nanomolar detection of Co^{2+}. This hypothesis is also supported by DFT optimization data. Assembly **2** was investigated for cation recognition properties, and it was found that the decoration of the organic receptor on the surface of ZnO makes the system selective for a particular metal ion. The successive addition of Co^{2+} to the solution of the sensor quenches the fluorescence intensity at 445 nm with enhancement at 353 nm. This leads to the development of a ratiometric fluorescence sensor for the recognition of Co^{2+} in a semi-aqueous solvent system with a detection limit of 0.4 nM. The strategy has the advantage to enhance the selectivity of receptors.

ASSOCIATED CONTENT

Supporting Information

Possible modes of binding between ZnO and receptor **1**, comparison of literature reported sensors with the present work, and optimization parameters of **1**, **2**, and ZnO. ^1H NMR, ^{13}C NMR, FTIR, solid state absorption, and emission spectra of receptor **1** and **2**. SEM and EDAX analysis of receptor **2**, after heating at 500 °C for 1 h, and the Co^{2+} complex of **2**. This

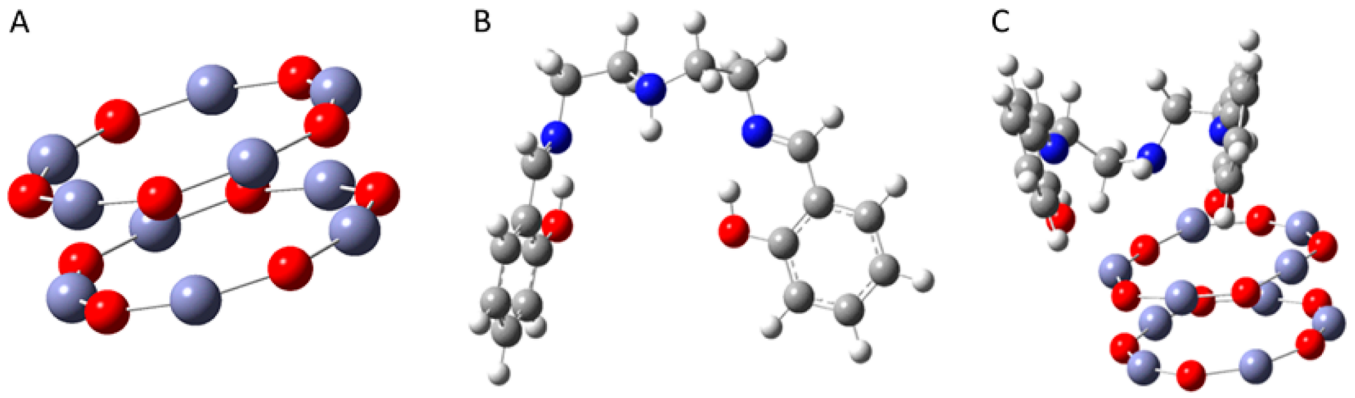

Figure 5. DFT optimized geometries of (A) ZnO, (B) receptor **1**, and (C) receptor **2** calculated from the B3LYP/6-311G basis set on Gaussian 09 program. Light blue spheres represent zinc. Gray spheres represent carbon. Bright blue spheres represent nitrogen. Red spheres represent oxygen. White spheres represent hydrogen.

material is available free of charge via the Internet at http://pubs.acs.org.

AUTHOR INFORMATION

Corresponding Authors

*E-mail: nsingh@iitrpr.ac.in (N.S.). Phone: +91-1881-242176 (N.S.).

*E-mail: navneetkaur@pu.ac.in (N.K.). Phone: +91-1722534464 (N.K.).

Author Contributions

The manuscript was written through contributions of all authors. All authors have given approval to the final version of the manuscript.

Notes

The authors declare no competing financial interest.

ACKNOWLEDGMENTS

This work was supported by CSIR Research Poject [01(2417)/10/EMR-11]. H.S. is thankful to IIT Ropar for a fellowship.

REFERENCES

(1) Desvergne, J. P., Czarnik, A. W., Eds.; *Chemosensors for Ion and Molecule Recognition*; Kluwer Academic Publishers: Dordrecht, The Netherlands, 1997.

(2) Li, M.; Gou, H.; Al-Ogaidi, I.; Wu, N. Nanostructured sensors for detection of heavy metals: A review. *ACS Sustainable Chem. Eng.* **2013**, *1*, 713−723.

(3) Thiele, D. J.; Gitlin, J. D. Assembling the pieces. *Nat. Chem. Biol.* **2008**, *4*, 145−147.

(4) McRae, R.; Bagchi, P.; Sumalekshmy, S.; Fahrni, C. J. In situ imaging of metals in cells and tissues. *Chem. Rev.* **2009**, *109*, 4780−4827.

(5) Sigel, H., Ed.; *Metal Ions in Biological Systems*; Marcel Dekker: New York, 1981; Chapter 12.

(6) De Silva, A. P.; Moody, T. S.; Wright, G. D. Fluorescent PET (photoinduced electron transfer) sensors as potent analytical tools. *Analyst* **2009**, *134*, 2385−2393.

(7) Basabe-Desmonts, L.; Reinhoudt, D. N.; Crego-Calama, M. Design of fluorescent materials for chemical sensing. *Chem. Soc. Rev.* **2007**, *36*, 993−1017.

(8) Asok, A.; Gandhi, M. N.; Kulkarni, A. R. Enhanced visible photoluminescence in ZnO quantum dots by promotion of oxygen vacancy formation. *Nanoscale* **2012**, *4*, 4943−4946.

(9) Asefa, T.; Duncanc, C. T.; Sharma, K. K. Recent advances in nanostructured chemosensors and biosensors. *Analyst* **2009**, *134*, 1980−1990.

(10) Li, R.; Luan, Y.; Zou, H.; Du, J.; Mud, T.; Li, Z. Synthesis and gas-sensing properties of ZnO particles from an ionic liquid precursor. *RSC Adv.* **2012**, *2*, 3049−3056.

(11) Barreca, D.; Bekermann, D.; Comini, E.; Devi, A.; Fischer, R. A.; Gasparotto, A.; Maccato, C.; Sada, C.; Sberveglieri, G.; Tondello, E. Urchin-like ZnO nanorod arrays for gas sensing applications. *CrystEngComm* **2010**, *12*, 3419−3421.

(12) Kaur, S.; Kaur, A.; Kaur, N. ZnO nanoparticles decorated with organic anion receptor: Selective recognition of sulfate anion. *Mater. Lett.* **2013**, *100*, 19−22.

(13) Kaur, K.; Kaur, N.; Singh, N. Imine coupled ZnO based fluorescent chemosensor for the simultaneous estimation of Al^{3+} and Cr^{3+}. *Mater. Lett.* **2012**, *80*, 78−80.

(14) Sharma, H.; Kaur, N.; Pandiyan, T.; Singh, N. Surface decoration of ZnO nanoparticles: A new strategy to fine tune the recognition properties of imine linked receptor. *Sens. Actuators, B* **2012**, *166−167*, 467−472.

(15) Sharma, H.; Narang, K.; Singh, N.; Kaur, N. Imine linked chemosensors coupled with ZnO: Fluorescent and chromogenic detection of Al^{3+}. *Mater. Lett.* **2012**, *84*, 104−106.

(16) Wang, X.; Summers, C. J.; Wang, Z. L. Large-scale hexagonal-patterned growth of aligned ZnO nanorods for nano-optoelectronics and nanosensor arrays. *Nano Lett.* **2004**, *4*, 423−426.

(17) Cho, S.; Jung, S.-H.; Lee, K.-H. Morphology-controlled growth of ZnO nanostructures using microwave irradiation: From basic to complex structures. *J. Phys. Chem. C* **2008**, *112*, 12769−12776.

(18) Tang, X.; Choo, E. S. G.; Li, L.; Ding, J.; Xue, J. One-pot synthesis of water-stable ZnO nanoparticles via a polyol hydrolysis route and their cell labeling applications. *Langmuir* **2009**, *25*, 5271−5275.

(19) Raula, M.; Rashid, Md. H.; Paira, T. K.; Dinda, E.; Mandal, T. K. Ascorbate-assisted growth of hierarchical ZnO nanostructures: sphere, spindle, and flower and their catalytic properties. *Langmuir* **2010**, *26*, 8769−8782.

(20) Singh, A. K.; Viswanath, V.; Janu, V. C. Synthesis, effect of capping agents, structural, optical and photoluminescence properties of ZnO nanoparticles. *J. Lumin.* **2009**, *129*, 874−878.

(21) Cozzoli, P. D.; Curri, M. L.; Agostiano, A.; Leo, G.; Lomascolo, M. ZnO nanocrystals by a non-hydrolytic route: Synthesis and characterization. *J. Phys. Chem. B* **2003**, *107*, 4756−4762.

(22) Liu, B.; Zeng, H. C. Hydrothermal synthesis of ZnO nanorods in the diameter regime of 50 nm. *J. Am. Chem. Soc.* **2003**, *125*, 4430−4431.

(23) Salimian, A.; Fern, G. R.; Withnalla, R.; Silver, J. A novel method for the preparation of non-agglomerated nanometre sized particles of lanthanum phosphate phosphors utilising a high surface area support in the firing process. *J. Mater. Chem.* **2012**, *22*, 21529−21532.

(24) Weintraub, B.; Zhou, Z.; Lib, Y.; Deng, Y. Solution synthesis of one-dimensional ZnO nanomaterials and their applications. *Nanoscale* **2010**, *2*, 1573−1587.

(25) Kim, M. J.; Kaur, K.; Singh, N.; Jang, D. O. Benzimidazole-based receptor for Zn^{2+} recognition in a biological system: a chemosensor operated by retarding the excited state proton transfer. *Tetrahedron* **2012**, *68*, 5429−5433.

(26) Joseph, R.; Chinta, J. P.; Rao, C. P. Lower rim 1,3-diderivative of calix[4]arene-appended salicylidene imine (H_2L): Experimental and computational studies of the selective recognition of H_2L toward Zn^{2+} and sensing phosphate and amino acid by [ZnL]. *J. Org. Chem.* **2010**, *75*, 3387−3395.

(27) Patterson, A. L. The Scherrer formula for X-ray particle size determination. *Phys. Rev.* **1939**, *56*, 978−982.

(28) Puri, J. K.; Singh, R.; Chahal, V. K.; Sharma, R. P. Novel hexacoordinate organosilicon(IV) complexes of diethylenetriamine Schiff base with SiO_2N_3 skeleton. *ARKIVOC* **2009**, *xi*, 247−256.

(29) Khullar, P.; Singh, V.; Mahal, A.; Dave, P. N.; Thakur, S.; Kaur, G.; Singh, J.; Kamboj, S. S.; Bakshi, M. S. Bovine serum albumin bioconjugated gold nanoparticles: Synthesis, hemolysis, and cytotoxicity toward cancer cell lines. *J Phys. Chem. C* **2012**, *116*, 8834−8843.

(30) Khullar, P.; Mahal, A.; Singh, V.; Banipal, T. S.; Kaur, G.; Bakshi, M. S. How PEO-PPO-PEO triblock polymer micelles control the synthesis of gold nanoparticles: Temperature and hydrophobic effects. *Langmuir* **2010**, *26*, 11363−11371.

(31) Bakshi, M. S.; Sachar, S.; Kaur, G.; Bhandari, P.; Kaur, G.; Biesinger, M. C.; Possmayer, F.; Petersen, N. O. Dependence of crystal growth of gold nanoparticles on the capping behavior of surfactant at ambient conditions. *Cryst. Growth Des.* **2008**, *8*, 1713−1719.

(32) Margelefsky, E. L.; Zeidan, R. K.; Davis, M. E. Cooperative catalysis by silica-supported organic functional groups. *Chem. Soc. Rev.* **2008**, *37*, 1118−1126.

(33) Valle, K.; Belleville, P.; Pereira, F.; Sanchez, C. Hierarchically structured transparent hybrid membranes by in situ growth of mesostructured organosilica in host polymer. *Nat. Mater.* **2006**, *5*, 107−111.

(34) Powers, K. W.; Brown, S. C.; Krishna, V. B.; Wasdo, S. C.; Moudgil, B. M.; Roberts, S. M. Research strategies for safety evaluation of nanomaterials. Part VI. Characterization of nanoscale particles for toxicological evaluation. *Toxicol. Sci.* **2006**, *90*, 296−303.

(35) Murdock, R. C.; Braydich-Stolle, L.; Schrand, A. M.; Schlager, J. J.; Hussain, S. M. Characterization of nanomaterial dispersion in

solution prior to in vitro exposure using dynamic light scattering technique. *Toxicol. Sci.* **2008**, *101*, 239−253.
(36) Straumal, B. B.; Mazilkin, A. A.; Protasova, S. G.; Myatiev, A. A.; Straumal, P. B.; Schutz, G.; van Aken, P. A.; Goering, E.; Baretzky, B. Magnetization study of nanograined pure and Mn-doped ZnO films: Formation of a ferromagnetic grain-boundary foam. *Phys. Rev. B* **2009**, *79*, 205206−205211.
(37) Straumal, B. B.; Myatiev, A. A.; Straumal, P. B.; Mazilkin, A. A.; Protasova, S. G.; Goering, E.; Baretzky, B. Grain boundary layers in nanocrystalline ferromagnetic zinc oxide. *JETP Lett.* **2010**, *92*, 396−400.
(38) Straumal, B. B.; Mazilkin, A. A.; Protasova, S. G.; Myatiev, A. A.; Straumal, P. B.; Goering, E.; Baretzky, B. Grain boundary layers in nanocrystalline ferromagnetic zinc oxide. *Thin Solid Films* **2011**, *520*, 1192−1194.
(39) Hou, J.; Chan, H.-Y.; Zhang, S.; Li, G.; Yang, Y. Synthesis, characterization, and photovoltaic properties of a low band gap polymer based on silole-containing polythiophenes and 2,1,3-benzothiadiazole. *J. Am. Chem. Soc.* **2008**, *130*, 16144−16145.
(40) Dijken, A. V.; Meulenkamp, E. A.; Vanmaekelbergh, D.; Meijerink, A. The kinetics of the radiative and nonradiative processes in nanocrystalline ZnO particles upon photoexcitation. *J. Phys. Chem. B.* **2000**, *104*, 1715−1723.
(41) Slavik, J. *Fluorescent Proves in Cellular and Molecular Biology*; CRC Press: Boca Raton, FL, 1994.
(42) Little, C.; Aakre, S. E.; Rumsby, M. G.; Gwarsha, K. Effect of Co^{2+}-substitution on the substrate specificity of phospholipase C from Bacillus cereus during attack on two membrane systems. *Biochem. J.* **1982**, *207*, 117−121.
(43) Dennis, M.; Kolattukudy, P. E. A cobalt-porphyrin enzyme converts a fatty aldehyde to a hydrocarbon and CO. *Proc. Natl. Acad. Sci. U.S.A.* **1992**, *89*, 5306−5310.
(44) Walker, K. W.; Bradshaw, R. A. Yeast methionine amino-peptidase I can utilize either Zn^{2+} or Co^{2+} as a cofactor: A case of mistaken identity. *Protein Sci.* **1998**, *7*, 2684−2687.
(45) Stoica, A. I.; Peltea, M.; Baiulescu, G. E.; Ionica, M. Determination of cobalt in pharmaceutical products. *J. Pharm. Biomed. Anal.* **2004**, *36*, 653−656.
(46) Patel, U. B.; Mehta, V. N.; Mungara, A. K.; Kailasa, S. K. 4-Aminothiophenol functionalized gold nanoparticles as colorimetric sensors for the detection of cobalt using UV−Visible spectrometry. *Res. Chem. Intermed.* **2013**, *39*, 771.
(47) Mehta, V. N.; Mungara, A. K.; Kailasa, S. K. Dopamine dithiocarbamate functionalized silver nanoparticles as colorimetric sensors for the detection of cobalt ion. *Anal. Methods* **2013**, *5*, 1818−1822.
(48) Zhang, M.; Liu, Y. Q.; Ye, B. C. Colorimetric assay for parallel detection of Cd^{2+}, Ni^{2+} and Co^{2+} using peptide-modifiedgold nanoparticles. *Analyst* **2012**, *137*, 601−607.
(49) Leng, Y.; Zhang, F.; Zhang, Y.; Fu, X.; Weng, Y.; Chen, L.; Wu, A. A rapid and sensitive colorimetric assay method for Co^{2+} based on the modified Au nanoparticles (NPs): Understanding the involved interactions from experiments and simulations. *Talanta* **2012**, *94*, 271−277.
(50) Zhang, F.; Zeng, L.; Zhang, Y.; Wang, H.; Wu, A. A colorimetric assay method for Co^{2+} based on thioglycolic acid functionalizedhexadecyl trimethyl ammonium bromide modified Au nanoparticles (NPs). *Nanoscale* **2011**, *3*, 2150−2154.
(51) Yao, Y.; Tian, D.; Li, H. Cooperative binding of bifunctionalized and click-synthesized silver nanoparticles for colorimetric Co^{2+} sensing. *ACS Appl. Mater. Interfaces* **2010**, *2*, 684−690.
(52) Kumar, P.; Shim, Y.-B. A novel cobalt(II)-selective potentiometric sensor based on *p*-(4-*n*-butylphenylazo)calix[4]arene. *Talanta* **2009**, *77*, 1057−1062.
(53) Li, C.-Y.; Zhang, X.-B.; Jin, Z.; Han, R.; Shen, G.-L.; Yu, R.-Q. A fluorescent chemosensor for cobalt ions based on a multi-substituted phenol-ruthenium(II) tris(bipyridine) complex. *Anal. Chim. Acta* **2006**, *580*, 143−148.
(54) Cannizzaro, V.; Bowie, A. R.; Sax, A.; Achterberg, E. P.; Worsfold, P. J. Determination of cobalt and iron in estuarine and coastal waters using flow injection with chemiluminescence detection. *Analyst* **2000**, *125*, 51−57.
(55) Vereda, E.; Rios, A.; Valcarcel, M. Simultaneous automatic determination of trace amounts of copper and cobalt by use of a flow-through sensor and first-derivative spectrometry. *Analyst* **1997**, *122*, 85−88.
(56) Tan, Y.; Yu, J.; Cui, Y.; Yang, Y.; Wang, Z.; Hao, X.; Qian, G. A novel 2,6-dicarbonylpyridine-based fluorescent chemosensor for Co^{2+} with high selectivity and sensitivity. *Analyst* **2011**, *136*, 5283−5286.
(57) Mori, I.; Takasaki, K.; Fujita, Y.; Matsuo, T. Selective and sensitive fluorometric determinations of cobalt(II) and hydrogen peroxide with fluorescein-hydrazide. *Talanta* **1998**, *47*, 631−754.
(58) Jung, H. J.; Singh, N.; Lee, D. Y.; Jang, D. O. Benzimidazole-based ratiometric fluorescent receptor exhibiting molecular logic gate for Cu^{2+} and Fe^{3+}. *Tetrahedron Lett.* **2009**, *50*, 5555−5558.
(59) Joshi, P.; Shewale, V.; Pandey, R.; Shanker, V.; Hussain, S.; Karna, S. P. Site specific interaction between ZnO nanoparticles and tryptophan: A first principles quantum mechanical study. *Phys. Chem. Chem. Phys.* **2011**, *13*, 476−479.
(60) Chang, J.; Waclawik, E. R. Experimental and theoretical investigation of ligand effects on the synthesis of ZnO nanoparticles. *J. Nanopart. Res.* **2012**, *14*, 1012−1023.
(61) Lee, C.; Yang, W.; Parr, R. G. Development of the Colle-Salvetti correlation-energy formula into a functional of the electron density. *Phys. Rev. B.* **1988**, *37*, 785−789.